Subinertial Frequency Response of Wind-Driven Currents in the Mixed Layer Measured by Drifting Buoys in the Midlatitude North Pacific

GERARD J. MCNALLY, DOUGLAS S. LUTHER AND WARREN B. WHITE

Scripps Institution of Oceanography, University of California, San Diego, La Jolla, California

(Manuscript received 29 October 1987, in final form 17 August 1988)

ABSTRACT

Previous analyses of satellite-tracked drifting buoy data (30 m drogue depth) and Fleet Numerical Ocean Center (FNOC) surface wind stresses in the midlatitude North Pacific during autumn/winter have shown near-surface current vectors consistently directed ~25° to the right of the surface wind stress vector (i.e., approximately parallel to sea level air pressure isobars). In the present study, the complex coherence between time series of the two vectors, near-surface current and surface wind stress, is examined using the vector cross-spectral analysis technique developed by Mooers, yielding the frequency response of surface current to wind stress from the inertial frequency down to one cycle per 16 days. The analysis shows that during summer the near-surface current is only weakly coherent with the surface wind stress, which coherence occurs at periods greater than a few days. In this season, the rotary spectrum of the near-surface current is dominated by anticyclonic motion, with periods of approximately 8 to 32 days, that is not locally wind-forced. In contrast, during autumn/winter, the two vectors are highly coherent over the subinertial frequency range corresponding to periods of 1 to 16 days. The phase estimates provided by vector cross-spectral analysis yield information on both the mean spatial angle and mean temporal phase difference between the major axes of the two ellipses described by the vector motions. Over the same subinertial frequency range where the coherence amplitude is significant, the average spatial angle between the major axis of the wind stress and the major axis of the near-surface current varies from 75° at the near-inertial frequencies to 15° at the low frequencies. The sign of the spatial angle is such that the near-surface current vector is always directed to the right of the surface wind stress vector. The temporal phase differences between the vectors show that the near-surface current vector lags the surface wind stress vector by 20° to 30° at near-inertial frequencies, diminishing to zero degrees with decreasing frequency. These phase lags correspond to temporal lags of up to four hours.

1. Introduction

The most persistent characteristic of the observations of near-surface, wind-driven, current vectors derived from the positions of satellite-tracked drifting buoys (drifters) is the angle between the direction of these current vectors and that of the surface wind stress vectors. Comparison of five-day averaged vectors of current from drifters drogued at 30 m depth and surface wind stress showed the former to be directed 15° to 35° to the right of the latter's direction (McNally 1981; McNally and White 1985). This result was based on observations made in the eastern midlatitude North Pacific—a region of weak geostrophic current (Wyrtki 1975) and large annual cycle in synoptic storm activity—during the season of strongest synoptic storm activity (i.e., autumn/winter). However, this measured angle between the trajectories of quasi-Lagrangian drifters and the surface wind is neither unique to drifting buoys nor to the specific configuration of drifting buoys used for these observations.

Nansen (1902) first reported observing a systematic angular difference between the wind direction and the surface current, based upon the movement of sea ice in the Arctic. He found that the surface current vector was ~26° to the right of the wind vector. These observations led Ekman (1905) to develop his classical theory of wind-driven currents. Zubov (1947) confirmed Nansen's finding, based on two years of similar Arctic observations. In addition, Zubov determined that ice drift occurred along the isobars of sea level air pressure averaged over five days. The same angular relationship between the direction of surface wind and current has been reported by other investigators using different drifting buoy configurations: Emery et al. (1985) in the Gulf of Alaska; and Peterson (1985) whose data indicated flow 26° to the left of the wind, south of the Straits of Magellan in the Southern Ocean.

In a more comprehensive study of wind-driven currents using drifters, McNally and White (1985) have established that near-surface wind-driven currents are: (i) nearly uniform over the mixed-layer depth, attenuating into the upper portion of the main pycnocline; (ii) have a crosswind component (i.e., normal to the wind-stress vector) in excellent agreement with an Ekman slab model, the latter accounting for ~85% of

Corresponding author address: Dr. Douglas S. Luther, Mail Code A-030, Scripps Institution of Oceanography, La Jolla, CA 92093.

the observed crosswind displacement at 30 m during autumn/winter; and (iii) have a downwind component that does not correlate at all with the wind stress at zero time lag, but exhibits a strong maximum correlation with the wind stress at the 6- to 12-hour time lag.

All of these observations in McNally and White (1985) were based on a time average of the surface wind stress and near-surface current vectors, providing no insight into the frequency dependence, if any, of the relationship between the surface wind stress and near-surface current vectors. However, an analysis technique does exist, developed by Mooers (1970, 1973), that enables the determination of the coherent spatial and temporal relationship between two, 2-dimensional, vectors as a function of frequency. The technique, which we will call vector cross-spectral analysis (or VCSA), is based upon the cross-spectral analysis of the rotationally invariant, rotary spectral components of the two vectors. Being a spectral methodology, it requires a large number of records that can be averaged in an ensemble sense to provide statistically meaningful results. The NORPAX drifting buoy dataset, when merged with the surface wind analyses of the Fleet Numerical Ocean Center (FNOC), provides ~7000 buoy days (~20 years) of observations, realizing the necessary degrees of freedom required for VCSA.

Section 2 briefly describes the data used in this study and reviews the VCSA technique. Some previous applications of VCSA to the study of wind-forced surface currents are also discussed. Section 3 describes the results of the present analyses, with an emphasis on the rotary spectral structure of the surface winds and currents, and the coherent relationships between them. Section 4 discusses the implications of the results presented in Section 3. An important caveat must be kept in mind whenever drifting buoy data are used to study ocean physics, i.e., that it is necessary to assume that the physical processes under study are invariant over the spatial domain covered by the drifters, which in this case is 30° to 55°N, 170° to 135°W. There is no reason to suspect, however, that the observed wind-current relationships are not representative of the entire domain from which data was collected for this study.

2. Data and methods

a. Data

The estimates of near-surface velocity used in this study were computed from the trajectories of 63 satellite-tracked drifters, drogued at 30 m in the mixed layer, and deployed in the midlatitude eastern North Pacific. These drifting buoys were all of the same design consisting of a cylindrical flotation element, 50 cm in diameter and 3 m in length, ballasted so as to float upright with one meter of the flotation element extending above the sea surface. The flotation elements for the RAMS (ARGOS) drifters were drogued by means of an 8.5 (4.3) meter diameter parachute at the end of a 30-meter drogue line (McNally et al. 1978). Drifters that lost their drogues were excluded from this study. Data were collected during the period June 1976 through June 1981. The majority (i.e., 51 of 55) of the drifting buoys were tracked by means of the Random Access Measurement System (RAMS), the precursor of the current ARGOS tracking system. There were two significant improvements made in the transition from the RAMS to the ARGOS system. First, the ARGOS system uses two satellites rather than the one satellite used by RAMS; and, second, the ARGOS system employs precisely located reference platforms whose exact positions are used to provide a system-wide correction to the navigational fixes of the nonreference platforms being tracked. Thus, the ARGOS system provides twice the number of platform locations per day than was available from RAMS, with a root mean square position error of less than 1 kilometer compared to the 5 kilometer position error afforded by RAMS. The raw positions of both RAMS and ARGOS data were first edited to remove "bad" data points, i.e., position fixes were rejected if they produced jumps in the raw velocities of greater than 75 cm s^{-1}. The edited positions were differenced to produce velocities which were then vector-averaged. The RAMS data yielded a position at noon UTC and one velocity per day, while ARGOS yielded four positions and velocities per day at the synoptic reporting intervals (000, 0600, 1200 and 1800 hours UTC).

The surface wind stress vectors for this study were derived from the Fleet Numerical Ocean Center's synoptic surface wind analyses that are available every six hours on approximately a 300 km × 300 km grid at midlatitudes. These wind data were linearly interpolated to the positions and times of the satellite fixes for each drifter, and then averaged in a manner commensurate with the averaging of the drifter data. For the purposes of this study, the wind velocity was converted to wind stress using the standard bulk formula (Fissel et al. 1977).

The resulting datasets, one for ARGOS and one for RAMS, were stratified by season since previous studies (e.g., McNally 1981) of subsets of these data in the time–space domain had shown a significant difference in the relationship between the wind-driven, near-surface currents and the surface wind stress in different seasons. Drifter data from the months of June through September were combined, regardless of year, to form a summer dataset. In the same manner, data collected during the months of November through April, again independent of year, were combined to form an autumn/winter dataset. A total of 104 and 132 thirty-two day records were provided by the RAMS drifters for the summer and winter periods, respectively. This daily RAMS data is used to study fluctuations at pe-

riods of 2 to 32 days. The ARGOS dataset is not nearly as large as that of the RAMS dataset. In order to achieve a comparable number of records for this study, the record length had to be considerably shortened; however, the sampling rate of four times a day provided a significant broadening of the frequency range over which the study was conducted. The ARGOS data can be used to study fluctuations at periods of 0.5 to 8 days, although only the subinertial band (1–8 days) is emphasized in this paper. In all, 122 eight-day records were available from ARGOS for the autumn/winter period. The ARGOS drifting buoys were deployed in August and had an average lifetime of nine months. These drifters provided only 24 eight-day ARGOS records for the summer period.

b. *Vector cross-spectral analysis*

Mooers (1970, 1973) developed a method for the cross-spectral analysis of pairs of two-dimensional vector time series (vector cross-spectral analysis, or VCSA), which is based on the decomposition of the vectors into polarized rotary components (i.e., clockwise and anticlockwise). The method provides a pair of complex-valued cross-covariances for the two vectors which result in an "inner" coherence amplitude and phase, $\gamma_{12}(\sigma)$ and $\chi_{12}(\sigma)$, and "outer" coherence amplitude and phase, $\lambda_{12}(\sigma)$ and $\phi_{12}(\sigma)$, which are all two-sided because they are defined over the frequency range $-\infty < \sigma < \infty$, where σ is the angular frequency of the rotating component and the sign of σ indicates the sense of rotation (i.e., $\sigma < 0$ clockwise, $\sigma > 0$ anticlockwise). The inner coherence amplitude and phase result from the cross-spectrum of the clockwise (anticlockwise) component of vector 1, and the clockwise (anticlockwise) component of vector 2. The outer coherence amplitude and phase result from the cross-spectrum of the clockwise (anticlockwise) component of vector 1 with the anticlockwise (clockwise) component of vector 2. Only the inner coherence amplitude and phase are used in this study.

Following Mooers (1973), the two-sided inner coherence amplitude, γ_{12}, and inner phase χ_{12} are

$$\gamma_{12}(\sigma) = \frac{|S_{w_1 w_2}|}{(S_{w_1 w_1} \cdot S_{w_2 w_2})^{1/2}}, \qquad -\infty < \sigma < \infty, \quad (2.1)$$

$$\chi_{12}(\sigma) = \tan^{-1}\left[\frac{-\mathrm{Im}(S_{w_1 w_2})}{\mathrm{Re}(S_{w_1 w_2})}\right], \qquad -\infty < \sigma < \infty, \quad (2.2)$$

where $w_1 = u + iv$ and $w_2 = \tau_x + i\tau_y$ are the complex representations of the two vectors; $S_{w_j w_j}$, $j = 1, 2$, are the real-valued inner-autospectra of each vector, respectively, and $S_{w_1 w_2}$ is the complex-valued, two-sided inner-cross-spectrum. Each of these spectra is readily defined in terms of the Co (C)- and Quad (Q)-spectra of the familiar one-sided autospectra and cross-spectra of the components of the near-surface velocity vector and wind stress vector:

$$S_{w_1 w_2}(\sigma) = \frac{1}{2}[(C_{u\tau_x} + C_{v\tau_y}) + (Q_{u\tau_y} - Q_{v\tau_x})] + \frac{i}{2}[-(Q_{u\tau_x} + Q_{v\tau_y}) + (C_{u\tau_y} - C_{v\tau_x})], \qquad -\infty < \sigma < \infty, \quad (2.3)$$

$$\left.\begin{aligned} S_{w_1 w_1}(\sigma) &= \tfrac{1}{2}[(C_{uu} + C_{vv}) + 2Q_{uv}], \qquad -\infty < \sigma < \infty \\ S_{w_2 w_2}(\sigma) &= \tfrac{1}{2}[(C_{\tau_x\tau_x} + C_{\tau_y\tau_y}) + 2Q_{\tau_x\tau_y}], \qquad -\infty < \sigma < \infty \end{aligned}\right\}. \quad (2.4)$$

Mooers goes on to show that the inner phase, χ_{12}, can be used to determine the mean angle $\Delta\alpha_{12}(\omega)$ between the major axes of the two ellipses described by the vector motions and the mean temporal phase difference $\Delta\beta_{12}(\omega)$:

$$\Delta\alpha_{12}(\omega) = \tfrac{1}{2}[\chi_{12}(\omega) + \chi_{12}(-\omega)], \quad (2.5)$$

$$\Delta\beta_{12}(\omega) = \tfrac{1}{2}[\chi_{12}(\omega) - \chi_{12}(-\omega)], \quad (2.6)$$

where $0 \leq \omega < \infty$.

This rather powerful and straightforward statistical technique for determining the coherence, phase, and angular differences as a function of frequency between a pair of two-dimensional vector time series is ideally suited for an investigation of the near-surface, wind-driven flow but has seen limited use, to date. This limited use can be traced to the paucity of current observations of long duration. Until recently, moored surface current meters were seldom deployed; rather, a subsurface flotation element has been used more frequently to provide the buoyancy necessary to maintain the upright position of still deeper current meters. This method was and is used to prevent contamination of the moored current meter measurements by noise due to the motions of the near-surface flotation devices induced by direct forcing by winds, waves, and/or near-surface currents. The subsurface flotation elements are usually set several hundred meters beneath the surface, thus precluding the collection of mixed-layer current meter measurements. Current meters specifically designed to operate near the surface on surface float moorings have been developed only recently (e.g., Weller and Davis 1980). Some of these have sufficient data records for a study of the wind-driven, near-surface currents using VCSA.

Gonella (1972) used VCSA in a study of the wind-driven near-surface currents measured from a 13-meter

deep current meter at Site D in the western North Atlantic. Only the summer and autumn data were used in his investigation, possibly in an effort to minimize the contaminating effects of mooring motions due to the higher winds and waves of the winter season. Gonella (1972) used five-day segments of the current meter record, thereby increasing the statistical significance of his result through ensemble averaging from a total of 52 five-day records. In discussing his results, Gonella (1972) made no distinction between the contributions of the spatial rotation and temporal phase lag to the inner coherence phase; rather, he interpreted $\chi_{12}(\sigma)$ (equal to $-\phi_w$ in his notation) as the total angle between the wind and current vectors, which he then compared to Ekman layer models. Using Gonella's estimates of $\chi_{12}(\sigma)$, values of $\Delta\alpha_{12}(\omega)$ and $\Delta\beta_{12}(\omega)$ have been calculated and plotted along with the complex coherence amplitude $\gamma_{12}(\sigma)$ and phase $\chi_{12}(\sigma)$ (Fig. 1). Significant coherence amplitude, between the wind vector and 13-meter current vector, is seen to have been limited to near-inertial frequencies (corresponding to periods of 1 to 5 days) and to be asymmetrical about zero frequency, displaying higher coherence between the clockwise (anticyclonic in the northern hemisphere) rotary components ($\sigma < 0$) than between the anticlockwise (cyclonic) rotary components ($\sigma > 0$). The decomposition of χ_{12} into the mean spatial angle $\Delta\alpha_{12}$ and the mean temporal phase $\Delta\beta_{12}$ in (2.5) and (2.6) reveals the temporal phase to have been approximately zero, with the spatial phase indicating that the current vector is directed approximately 90° to the right of the wind vector, in the 1–5 day band.

Use of the VCSA in the study of wind-driven, near-surface currents is also found in Davis et al. (1981) in analyses of near-surface current meter records from the Mixed-Layer Experiment (MILE). The data records from MILE are relatively short (~20 days), and were obtained in late summer. The coherence amplitude, γ_{12}, was found to be significant only for subinertial frequencies (corresponding to periods of about 1 to 4 days), but was symmetrical about zero frequency. The coherence phase indicated the wind-driven current at 5 meter depth to be directed approximately 90° to the right of the wind with approximately zero time lag.

The studies by Gonella (1972) and Davis et al. (1981) used Eulerian measures of the near-surface currents from moored current meters. More recently, Daniault et al. (1985) applied VCSA to Lagrangian measures of the wind-driven, near-surface current, having utilized undrogued drifters to obtain twenty-seven five-day segments during 16 August–27 November 1982. The coherence of these records with the wind stress was statistically significant only for subinertial frequencies (corresponding to periods of 1 to 5 days), but was more symmetrical about zero frequency than Gonella (1972) reported. The phase (Fig. 6 in Daniault et al. 1985) is quite different from that seen in either Gonella (1972) or Davis et al. (1981). If the results of Daniault et al. are reinterpreted in terms of (2.5) and (2.6), then for subinertial frequencies (corresponding to periods of 1 to 5 days) the average spatial angle, $\Delta\alpha_{12}$, is ~30° to the right of the wind, and the average temporal phase lag, $\Delta\beta_{12}$, is ~20° (corresponding to a lag of the current relative to the wind stress of approximately one hour for a period of one day, and 7 hours for a period of four days). (The relationships found between surface winds and currents discussed above, are summarized in Table 1.)

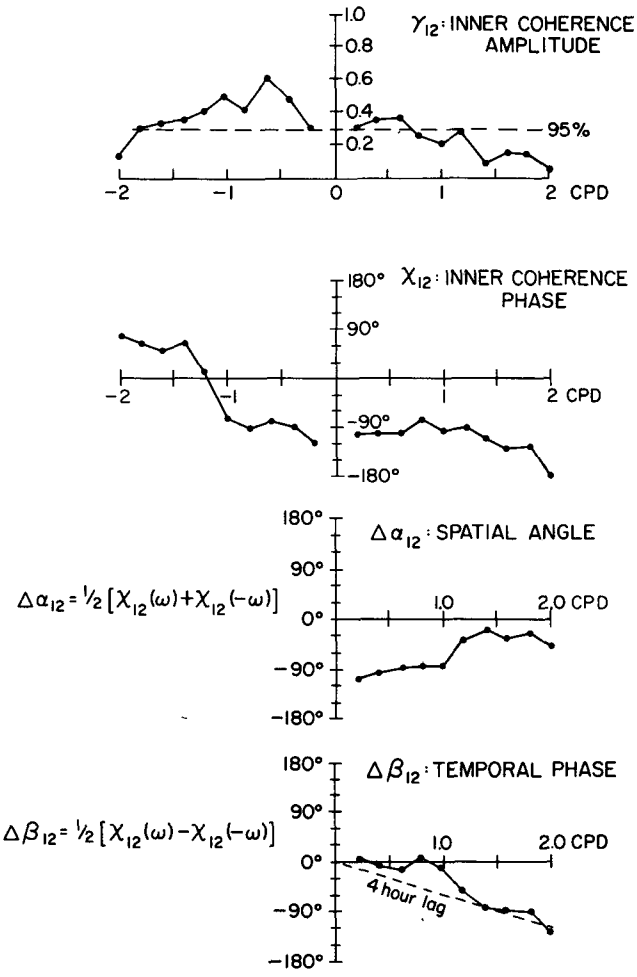

FIG. 1. Coherence amplitude, γ_{12}, and phase, χ_{12}, between surface wind stress and near-surface current, adapted from Gonella (1972, Fig. 8). The values of γ_{12}, have been used to compute the spatial angles, $\Delta\alpha_{12}$, and temporal phase lags, $\Delta\beta_{12}$, between the major axes of the wind stress and current vector motions. Gonella actually plots a phase he calls ϕ_w, the negative of which is equal to χ_{12}, as plotted here, where vector 1 is surface wind stress and vector 2 is near-surface current. The ordering of the vectors is that chosen by Gonella, and implies that a negative value of $\Delta\alpha_{12}$, indicates that the current vector is directed to the right of the wind, while a negative value of $\Delta\beta_{12}$, indicates that the wind lags the current. A four-hour lag would produce values of $\Delta\beta_{12}$ indicated by the dashed line. Note that, due to the small values of γ_{12} at frequencies greater than 1 cpd, the values of $\Delta\alpha_{12}$, and $\Delta\beta_{12}$, have dubious significance at these high frequencies.

TABLE 1. Approximate estimates of spatial angles,[a] $\Delta\alpha_{12}$ and temporal phase lags,[a] $\Delta\beta_{12}$ between the major axes of the near-surface current and wind stress vector ellipses, from this and previous studies.

Source	Time period	Depth of measured current (m)	Period band (days) 1–4 $\Delta\alpha_{12}$	1–4 $\Delta\beta_{12}$	4–16 $\Delta\alpha_{12}$	4–16 $\Delta\beta_{12}$
Gonella[b,c] (1972)	Summer/Fall	13	90° ± 12°	0° ± 12°	insignificant coherence	
Davis et al.[b] (1981)	19 Aug 1977–6 Sep 1977	5	90° ± 15°	0° ± 15°	not enough data to estimate	
Daniault et al.[b,c] (1981)	16 Aug 1982–27 Nov 1982	0–2	30° ± 9°	−20° ± 9°	not enough data to estimate	
This study	Summer (Jun–Sep)	30	not enough data to estimate		33° ± 10°	−1° ± 10°
This study	Winter (Nov–Apr)	30	60° ± 4°	−25° ± 4°	16° ± 4°	−2° ± 4°

[a] Vector 1 is near-surface current and vector 2 is surface wind stress, so that a positive value of $\Delta\alpha_{12}$ implies that the current vector is directed to the right of the wind stress vector, while a negative value of $\Delta\beta_{12}$ implies that the current lags the wind in time. Differing sign conventions for the coherence phase and opposite ordering of the vectors, in the papers cited, has been accounted for. Error bars are 95% limits.

[b] Phase estimates have been rounded to the nearest 10° due to the inaccuracy of extracting phases from figures in the referenced articles. Error estimates are our calculation of the 95% error bars based on information supplied in the respective articles.

[c] Estimates given for the 1–4 day band are actually estimates for the 1–5 day band.

3. Results of the present study

a. Rotary spectra

In addition to elucidating characteristics of the separate atmospheric and oceanic motions, rotary spectra of the surface wind stress and near-surface currents provide insight into the nature of the relationship between these vector time series. The rotary spectral energy density components are displayed in Fig. 2. The anticyclonic (dashed) and cyclonic (solid) spectra of the near-surface velocity vector, $\bar{v}$, and surface wind stress vector, $\bar{\tau}$, for summer and winter are shown in left and right panels, respectively, for the ARGOS drifters (top panels) and RAMS drifters (lower panels). Notice that the spectral slopes of the RAMS surface current data markedly change at around four days, tending to be flatter, or "whiter," at periods less than four days. This structure is not evident in the ARGOS spectra. Also, the RAMS spectra at periods less than four days show little polarization, while the ARGOS spectra are highly polarized. We conclude that the RAMS data, for periods shorter than four days, are strongly contaminated by measurement noise (i.e., satellite position fix errors). For the purpose of computing spectral energy densities, the RAMS (ARGOS) data were divided into 64-day (16-day) pieces, rather than the 32-day (8-day) pieces which are employed later in the coherence calculations that require more piece-wise averaging to improve statistical reliability.

The ARGOS surface current spectra (Fig. 2, top panel) are seen to be anticyclonically polarized (dashed lines) across nearly the entire frequency range that is computed, during both the summer and winter seasons. At lower frequencies (corresponding to periods of about 8 to 32 days), only the summer RAMS data (lower left panel) exhibit a clear tendency to be anticyclonically polarized, while there appears to be no rotational preference, or only a weak anticyclonic preference, in the winter RAMS data (lower right panel). The summer wind stress spectra exhibit a tendency toward anticyclonic polarization in approximately the 1- to 8-day band, while the winter wind stress spectra have a tendency toward anticyclonic polarization in only a narrow frequency band near the five-days period. These polarization characteristics of the surface current and wind stress fields can be more clearly visualized in plots of the ratio of anticyclonic spectral energy density to total spectral energy density (anticyclonic plus cyclonic), as in Fig. 3.

In Fig. 3 as for subsequent figures, the high-frequency range (periods shorter than four days) is obtained from the ARGOS data, since the RAMS data is clearly dominated by noise there, while the low-frequency range (periods longer than four days) is obtained from the RAMS data due to its higher statistical reliability. The polarization characteristics discussed above are clearly evident in Fig. 3. That is, 1) the predominance of anticyclonic motion of the summer surface currents (dashed lines) at periods shorter than four days and longer than about eight days (primarily 10 to 20 days), while the wind stress indicates a preference for anticyclonic polarization only at periods of about 1 to 8 days; 2) in the winter, at short periods (less than four days), the surface currents are again strongly anticyclonically polarized, while the wind stress shows no polarization preference; and 3) in the winter, at long periods (greater than four days), there is a tendency toward anticyclonic motion in surface current and wind

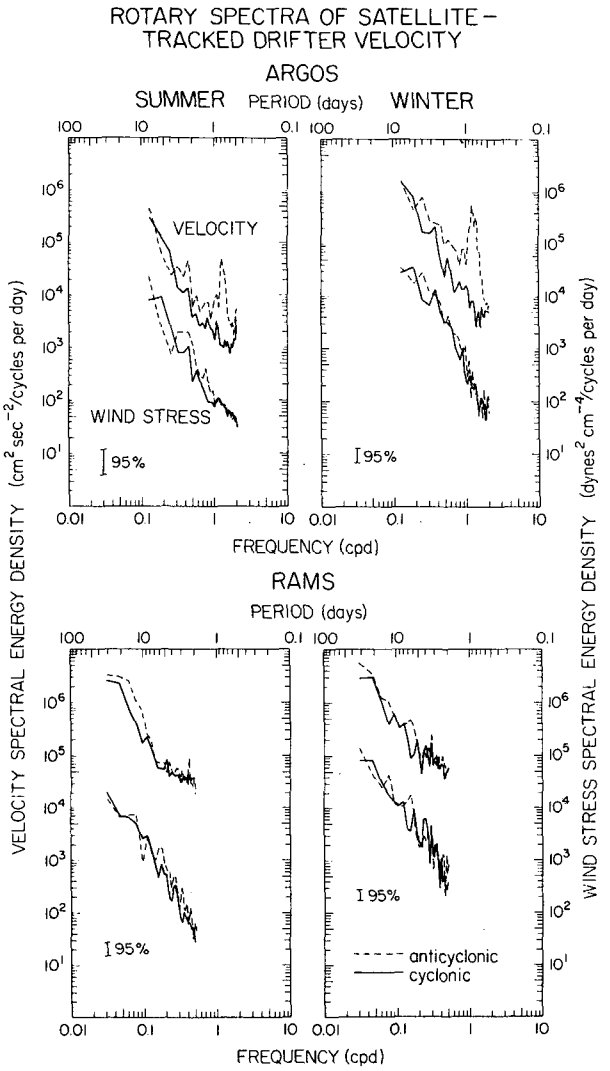

FIG. 2. The anticyclonic (dashed) and cyclonic rotary spectra of the near-surface current and wind stress vector time series. These spectra result from the ensemble averaging of: (top) 24 eight-day summer records and 122 eight-day winter records from the ARGOS dataset; and (bottom) 104 thirty-two day summer records and 132 thirty-two day winter records from the RAMS dataset.

stress only at about five to eight days, a period band usually associated with synoptic storm activity in the winter. This latter anticyclonic behavior suggests that the RAMS drifters were, on average, located on the south sides of the eastward moving winter cyclones (Price 1983). A remarkable feature of the low-frequency, winter spectral ratios in Fig. 3, that was not obvious from the spectra in Fig. 2, is the strong similarity of the surface current and wind stress plots, which suggests a high coherence between surface current and wind stress at low frequencies during the winter.

The ratio of the total spectral energy density (i.e., the sum of the anticyclonic plus cyclonic components) of the near-surface water velocity vector to that of the surface wind stress, as a function of frequency (Fig. 4), is high in the summer over the frequency range corresponding to periods of about 8 to 32 days. The summer ratio at near-inertial frequencies (the inertial frequency varies from 1.0 to 1.6 cpd for the drifter data) in the right panel is even higher, indicating the resonant nature of the oceanic response there. The winter ratio is essentially a constant, 0.4, over the entire frequency range corresponding to periods of 1 to 32 days, while a significant increase occurs above the average ratio of 0.4 at near-inertial frequencies.

The ratio of winter-to-summer total spectral energy densities for both the near-surface currents and surface wind stress, plotted as a function of frequency (Fig. 5), demonstrates that higher energy levels occur during the winter over most of the subinertial frequency range. Although both quantities generally exhibit an increase in spectral energy density from summer-to-winter, the increase is not a uniform function of frequency for either the near-surface velocity or wind stress vectors. While both show larger increases in the synoptic storm range, five- to eight-day periods, the increases are not of the same percentage. Notice the different ordinate scales for the ratios of the two vectors in the low frequency end provided by the RAMS drifting buoys (top panel). Therefore, in the frequency range for synoptic storms, a ten-fold increase occurs in the spectral energy density of the surface wind stress but only a four-fold increase occurs in the spectral energy density of the near-surface current. At the higher end of the subinertial frequency range provided by the ARGOS drifters, the ratio of both vectors have the same vertical scale. The resonant nature of the oceanic response at near-inertial frequencies is graphically demonstrated, where a 2.5 times increase in spectral energy density of the surface wind stress results in as much as a 35 times increase in the spectral energy density of the near-surface currents.

b. Complex coherence and phase

The complex coherence between the surface current (vector 1) and wind stress (vector 2) time series was calculated using the VCSA technique described earlier. The complex coherences for three drifting buoy datasets, Summer RAMS, Winter RAMS, and Winter ARGOS, are shown in Fig. 6. The complex coherence for the Summer RAMS dataset was computed from the ensemble average of rotary auto- and cross-spectra computed from 104 thirty-two day records. These records consisted of the near-surface velocity and surface wind stress from two summers, 1976 and 1977. The complex coherence for the Winter RAMS dataset was computed from an ensemble average of rotary spectra from 132 thirty-two day records from the winters of 1976/77 and 1977/78. The complex coherence for the

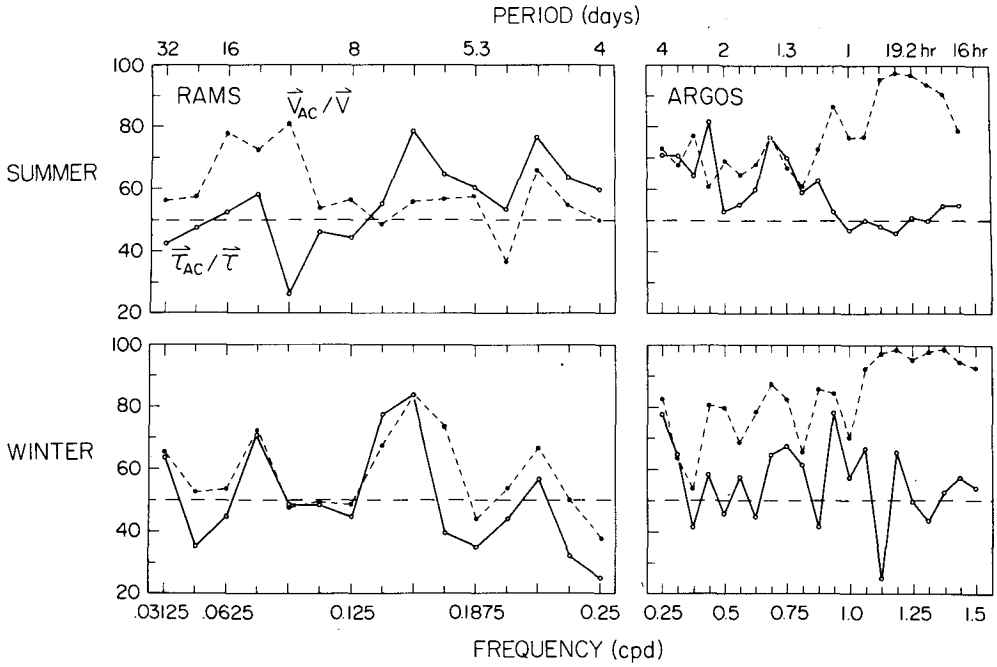

FIG. 3. Plots of the ratios (given as a percent) of each of the anticyclonic spectra in Fig. 2 divided by the total spectral energy densities (i.e., sum of anticyclonic and cyclonic spectra). The top panels show summer estimates and the bottom panels show winter estimates. For periods greater than 4 days, only estimates using RAMS data are used, while for periods less than 4 days, only the ARGOS estimates are reliable (see the text). Notice the different scales for the abscissas.

Summer RAMS dataset (Fig. 6, dashed lines) shows the near-surface velocity $\bar{v}$ to be only weakly coherent with the surface wind stress vector $\bar{\tau}$ over the frequency range corresponding to periods less than 32 days (but, recall that the RAMS data is noisy at periods less than 4 days). A sufficient number of Summer ARGOS records were not available to allow a statistically meaningful investigation of the complex coherence at near-inertial frequencies (i.e. periods less than 4 days).

The Winter RAMS data (Fig. 6, solid dotted lines) shows the near-surface velocity vector, $\bar{v}$, to be highly coherent with the surface wind stress vector, $\bar{\tau}$, over

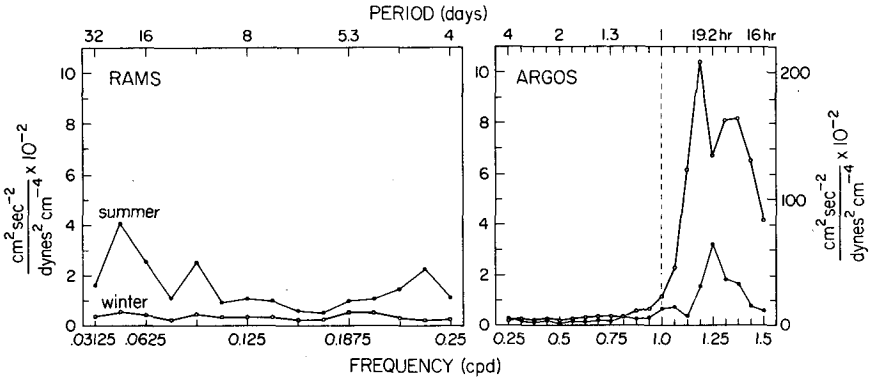

FIG. 4. The ratio of the total spectral energy density (anticyclonic plus cyclonic) of the near-surface current divided by the total spectral energy density of the surface wind stress is plotted as a function of frequency for the summer (solid dotted lines) and winter (open dotted lines) spectra of Fig. 2. As for Fig. 3, RAMS (ARGOS) data is employed for periods longer (shorter) than 4 days. The ordinate scale at far right applies only for frequencies greater than or equal to 1.0 cpd (that is, on and to the right of the dashed line); hence the ordinate range is 0 to 0.1 (cm s^{-1})^2/(dyn cm^{-2})^2 for frequencies less than 1.0 cpd, and 0 to 2.0 (cm s^{-1})^2/(dyn cm^{-2})^2 for frequencies greater than or equal to 1.0 cpd.

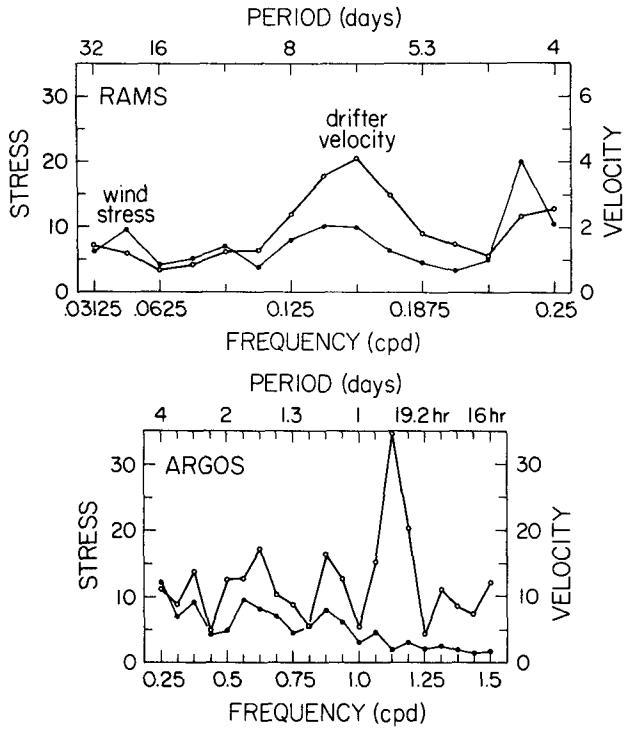

FIG. 5. The ratio of the total spectral energy density (anticyclonic plus cyclonic) in winter divided by the total spectral energy density in summer for near-surface currents (open dotted lines) and surface wind stress (solid dotted lines). As for Fig. 3, RAMS (ARGOS) data is employed for periods longer (shorter) than 4 days. Notice that the ordinate scale for surface current differs from the ordinate scale for wind stress in the upper panel, but not in the lower panel.

the entire frequency range except at periods shorter than three days where the large noise content of the RAMS data is apparently reducing the coherence amplitude. The complex coherence for the Winter ARGOS dataset was computed from 122 eight-day records from the winter of 1980/81. The combination of the Winter ARGOS and RAMS estimates of complex coherence show the near-surface velocity vector to be highly coherent with the surface wind stress vector over the entire 1–16 day band, with the coherence amplitude essentially symmetric about zero frequency (Fig. 6, upper panel). For the coherence phases (Fig. 6, lower panel), the estimates from the RAMS data at periods less than four days have been discarded, as in previous figures, due to the probable high noise content in this data at these periods. Furthermore, the individual phase estimates from the summer RAMS data are generally not significantly different from zero at the 95% level, and so are not plotted, although their mean value does contribute to the summary in Table 1. The phases for the Winter RAMS and Winter ARGOS data are not symmetric about zero frequency except at lower frequencies where they are $\sim 15°$. The anticyclonic ($\sigma < 0$) phase tends to be much larger than the cyclonic ($\sigma > 0$) phase. The 95% error bars for the plotted phases are nearly everywhere smaller than $\pm 13°$.

Combining the phase estimates in the manner prescribed in (2.5), provides estimates of the average spatial angle, $\Delta\alpha_{12}$, between the major axes of the two ellipses described by the motions of the $\bar{v}$ and $\bar{\tau}$ vectors. The average spatial angle, $\Delta\alpha_{12}$ (Fig. 7, upper panel), is seen to be fairly constant over the frequency range corresponding to periods of 4 to 16 days, with an average value of $\sim 15°$. A positive value of $\Delta\alpha_{12}$ indicates the near-surface current velocity vector, $\bar{v}$, is directed to the right of the surface wind stress vector, $\bar{\tau}$. Over the rest of the frequency range, corresponding to periods of 4 to 1.1 days, $\Delta\alpha_{12}$ increases reaching a maximum value of 76° at a period of 1.3 days. The average phase lag between the major axes of $\bar{v}$ and $\bar{\tau}$ [i.e., $\Delta\beta_{12}$ in (2.6)], is shown in the lower panel of Fig. 7, where

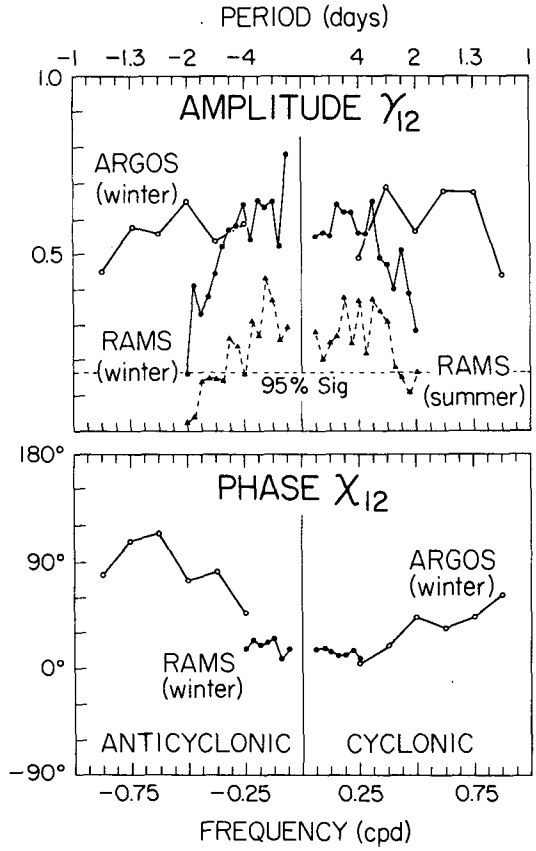

FIG. 6. The inner coherence amplitude (upper panel) and phase (lower panel) between near-surface current and surface wind stress. As in previous plots, the data are divided according to season and type of satellite tracking. ARGOS summer estimates of amplitude and phase, as well as RAMS summer estimates of phase, are not plotted due to their statistical unreliability (see text). The 95% level of no significance for summer RAMS amplitude estimates is shown as a dashed horizontal line in the upper panel, while the 95% levels for the remaining estimates are slightly lower. Nearly all the phase estimates plotted have 95% error bars smaller than $\pm 13°$.

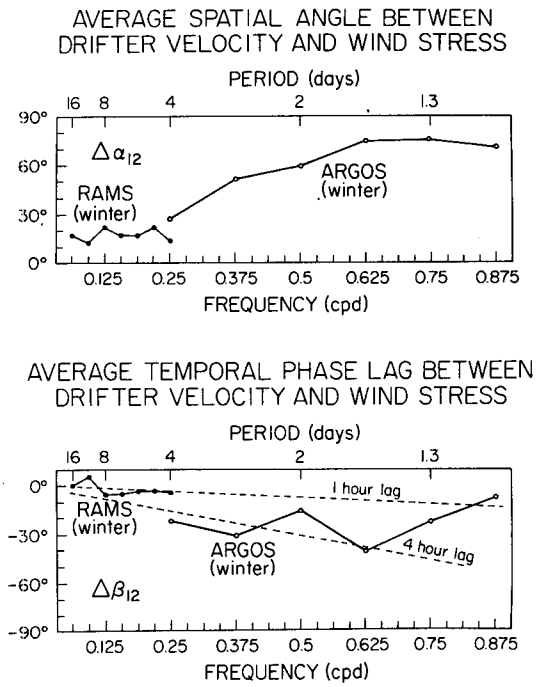

FIG. 7. The spatial angles, $\Delta\alpha_{12}$, and temporal phase lags, $\Delta\beta_{12}$, between the major axes of the current vector and wind stress ellipses. As for Fig. 3, RAMS (ARGOS) data is employed for periods longer (shorter) than four days. A positive value of $\Delta\alpha_{12}$ implies that the current vector is directed to the right of the wind stress vector. A negative value of $\Delta\beta_{12}$ implies that the current lags the wind. One and four-hour lags would produce values of $\Delta\beta_{12}$ indicated by the dashed lines.

values of $\Delta\beta_{12} < 0$ indicate that the near surface current vector $\bar{v}$ lags the surface wind stress vector $\bar{\tau}$. Here $\Delta\beta_{12}$ is seen to be fairly constant at low frequency with an average value indistinguishable from 0° for the frequency range corresponding to periods 4 to 16 days. For periods less than 4 days, $\Delta\beta_{12}$ first increases in magnitude, reaching a value of −40° at a period of 1.6 days, then decreases in magnitude reaching a value of −8° at a period of 1.1 days. These are all rather small lags in terms of time elapsed. The dashed lines in Fig. 7 show the phases expected for lags of 1 and 4 hours.

The approximate values of $\Delta\alpha_{12}$ and $\Delta\beta_{12}$ obtained from this study are summarized in Table 1 and compared there with the prior estimates discussed in section 2.

4. Discussion

Considering the disparity in the polarization of the summer wind stress vectors and near-surface velocity vectors (Fig. 3, upper panel), it is not surprising that the coherence (Fig. 6, Summer RAMS) would show the two vectors to be only weakly coherent during this period. The drifter trajectories for these summer data (not shown) indicate that the flow was dominated by mesoscale eddy activity, with radii of approximately 100 kilometers and rotation periods of approximately 30 days (e.g., see Fig. 7 of McNally 1981). The sign of rotation was chiefly anticyclonic as seen in the preferential polarization of the near-surface velocity vector in Fig. 3 (upper panel, left side) and Fig. 2 (lower panel, left side). The geostrophic mesoscale eddies have a greater influence on the near-surface currents measured by the drifters during summer partly because of the much weaker surface wind stress (hence, weaker directly-forced surface currents) in summer compared to winter, and partly because the 30 m drogue depth of the drifters is frequently beneath the seasonal thermocline (e.g., see Fig. 6 of McNally and White 1985). Above the seasonal thermocline, the currents might be expected to be somewhat more correlated with the wind stress. The weakly coherent nature of the current and wind stress vectors during summer at the low frequency end of the subinertial frequency range is in agreement with the lowest-frequency estimate of coherence in an earlier study conducted with moored current meter data (i.e., Gonella 1972). Unfortunately, for periods shorter than 4 days, the Summer RAMS data is not reliable and the Summer ARGOS data is too sparse, so we cannot confirm or contradict the findings of high coherence there reported by other authors (see Table 1).

The Winter RAMS and ARGOS datasets demonstrate the summer-to-winter difference in the response of the drifting buoys to the wind stress. The increase in spectral energy density in both $\bar{v}$ and $\bar{\tau}$ has been shown in Figs. 2 and 4. A reduction in mesoscale activity in $\bar{v}$ is found in the frequency range corresponding to periods of 10 to 32 days, associated with an increase in synoptic storm energy in $\bar{\tau}$ (Fig. 5), and there is a high degree of correlation in the polarization of both vectors (Fig. 3). Finally, there is the almost constant ratio of total spectral energy density of the near-surface velocity vector to surface wind stress vector (Fig. 4) with the exception of the resonant inertial response. All of these observations indicate that near-surface velocity vectors are strongly coupled to the forcing by surface wind stress in autumn/winter, but not in the summer except at near-inertial frequencies (periods less than 4 days) according to previous studies (section 2 and Table 1). The complex coherence between the near-surface current and surface wind stress vectors (Fig. 6) demonstrates in a rigorous fashion that the near-surface velocity and surface wind stress vectors are only weakly coherent in the summer at long periods but highly coherent in the autumn/winter.

The decomposition of the coherence phase into average spatial angle $\Delta\alpha_{12}$ and average temporal phase $\Delta\beta_{12}$ (Fig. 7) generally confirms the results of previous studies of subsets of these drifting buoy data (McNally 1981; McNally and White 1985), which indicated that 5- to 30-day averages of the two vectors found the near-

surface velocity vector directed 15° to 35° to the right of the surface wind stress vector (being smaller for the larger averaging interval), while lagging the wind stress vector by at most 6 hours. The present study formalizes and expands upon these results, finding an average spatial angle $\Delta\alpha_{12}$ of approximately 15°, with an average time lag of less than a few hours for the low frequencies (periods greater than 4 days); while at shorter periods, the spatial angle of the surface current relative to the wind grows to as much as 75° *cum sole* with the time lag rarely greater than 4 hours.

A definitive explanation for the wind-current relationships reported here is not available, and a full theoretical investigation of the possible causes is outside the scope of this paper. However, a few comments are in order. The first issue is whether the drifters are properly tagging water motion at 30 m depth, or whether they are significantly displaced by the effects of winds and waves on their surface-following hulls. Approximately one meter of the drifter hull is exposed to the wind, which results in a downwind force on the drifter that could produce substantial displacements (called "windage") if the wind is strong. Attempts to correct the movement of drifters (of the same design as those discussed here) for windage have not been successful, either overestimating the downwind movement of drogueless drifters (Kirwan et al. 1978), or underestimating the downwind movement of drifters with small drogues (McNally and White 1985). Both estimates were probably too high, since the latter used the FNOC winds analyzed for a height of 19.5 m as an approximation to the 1 m wind, while the former used a logarithmic law to reduce the FNOC 19.5 m winds to a 1 m level although it is well-known (Kraus 1967) that the log law overestimates the wind speed in the neighborhood of the surface roughness, that is, below wave crest height (it is likely that the crest-to-trough wave amplitudes exceed 1 m most of the time). Given the larger drogues of most of the drifters used in this study, it is difficult to imagine that windage can account for much of the low-frequency downwind displacement that is evidenced by Fig. 7, especially when there is no reason to expect a frequency dependence for the windage (note that the high frequency drifter movement is almost completely crosswind according to Fig. 7).

The response of a drifter's hull to the passage of surface waves can lead to mean forces on the drifter that are either in the direction of wave propagation or opposed to that direction (Davis et al. 1982). If the waves have been locally forced, this could lead to upwind or downwind drifter movement. Whether Davis et al.'s (1982) monochromatic laboratory results can be directly applied to open ocean conditions is unknown and would seem unlikely. Also unknown are the specific response characteristics of the drifters used here either for a monochromatic laboratory wave field or more general open ocean wave fields. However, neither waveage nor windage, nor some combination thereof, is consistent with the behavior of deeply drogued, but otherwise similar, drifters that McNally and White (1985) have discussed. They point out that drifters drogued at 60 and 90 m showed no downwind or upwind movement, despite the occurrence of strong wind events, until the mixed-layer depth became deeper than the drogue depth. McNally (1981) also found, using a subset of the data used here, that the five-day average angle between wind stress and surface current was not a function of wind stress magnitude, implying that windage and waveage appear unimportant.

Having argued that the drifters firmly tag the water at their nominal drogue depths of 30 m, the obvious explanation for the *cum sole* angle of the surface current relative to the wind stress arises from Ekman (1905). But Ekman's (1905) theory is insufficient to explain the small spatial angles at low frequencies, in combination with the large angles at high frequencies, in Fig. 7 (see, for instance, the summary of Ekman layers in Gonella 1972). McNally and White (1985) have shown that the crosswind movement of the drifters (partial data overlap with this study) at the longest periods is consistent with an Ekman slab model (Davis et al. 1981). One might then invoke Stokes drift, or a viscosity that increases with depth in an Ekman layer model (Madsen 1977) to account for the large downwind drifter movement at low frequencies, although the former shouldn't be important at 30 m and the latter still doesn't explain the frequency dependence of the spatial angle. Certainly, the possible role of forced baroclinic motions cannot be overlooked. The Ekman transport convergence/divergence patterns impressed upon the ocean by surface winds produce near-surface pressure patterns in the ocean that balance geostrophic flow in the direction of the wind (e.g., see Gill 1982, § 9.4 and § 9.11). Large baroclinic downwind currents can be generated that might explain the unexpectedly large downwind movement of the drifters at low frequency (White and McNally 1987). In fact, the White and McNally (1987) model shows that the ratio of the wind-forced, baroclinic response (downwind) to the Ekman mixed-layer response (crosswind) increases as frequency decreases from the inertial frequency, in agreement with Fig. 7. Unfortunately, however, the temporal phase lag of the baroclinic response to the wind stress in White and McNally (1987) is 90°, so that their model predicts increasing phase lag with decreasing frequency, which is in marked disagreement with Fig. 7.

Acknowledgments. This work was supported by NASA under Grant NAGW-664.

REFERENCES

Daniault, N., P. Blouch and F. X. Fusey, 1985: The use of free-drifting meteorological buoys to study winds and surface currents. *Deep-Sea Res.*, **32**, 107–113.

Davis, R. E., R. de Szoeke and P. Niiler, 1981: Variability in the upper ocean during MILE, Part II: Modeling and mixed-layer response. *Deep-Sea Res.*, **28A,** 1453–1475.

——, J. E. Dufour, G. J. Parks and M. R. Perkins, 1982: Two inexpensive current following drifters. S.I.O. Technical Report No. 82–28.

Ekman, V. W., 1905: On the influence of the earth's rotation on ocean-currents. *Arkiv. für Matematik, Astronomi och Fysik* 2, 52 pp.

Emery, W. J., T. C. Royer and R. W. Reynolds, 1985: The anomalous tracks of North Pacific drifting buoys 1981 to 1983. *Deep-Sea Res.*, **32,** 315–347.

Fissel, A., S. Pond and M. Miyaki, 1977: Computation of surface fluxes from climatological and synoptic data. *Mon. Wea. Rev.*, **105,** 26–36.

Gill, A. E., 1982: *Atmosphere-Ocean Dynamics,* Academic Press.

Gonella, J., 1972: A rotary-component method for analyzing meteorological and oceanographic vector time series. *Deep-Sea Res.*, **19,** 833–846.

Kirwan, A. D., G. McNally and S. Pazan, 1978: Wind drag and relative separations of undrogued drifters. *J. Phys. Oceanogr.*, **8,** 1146–1150.

Kraus, E. B., 1967: Wind stress along the sea surface. *Advances in Geophysics,* Vol. 12, Academic Press, 213–255.

Madsen, O. S., 1977: A realistic model of the wind-induced Ekman boundary layer. *J. Phys. Oceanogr.*, **7,** 248–255.

McNally, G. J., 1981: Satellite-tracked drift buoy observations of the near-surface flow in the eastern mid-latitude North Pacific. *J. Geophys. Res.*, **86,** 8022–8030.

——, E. Reyna, W. J. Merrell, Jr. and A. D. Kirwan, Jr., 1978: Technical evaluation of ADS I and II drifter performance. Tech. Rep. TAMU 78-3-7, Dept. of Oceanography, Texas A&M University.

——, and W. B. White, 1985: Wind-driven flow in the mixed layer observed by drifting buoys during autumn/winter in the mid-latitude North Pacific. *J. Phys. Oceanogr.*, **15,** 684–694.

Mooers, C. N. K., 1970: The interaction of an internal tide with the frontal zone in a coastal upwelling region, Ph.D. dissertation, Oregon State University, 480 pp.

——, 1973: A technique for the cross spectrum analysis of pairs of complex-valued time series, with emphasis on properties of polarized components and rotational invariants. *Deep-Sea Res.*, **20,** 1129–1141.

Nansen, F., 1902: The oceanography of the North Polar Basin. Scientific results of the Norwegian North Polar Expedition, 1893–1896. **9,** 427 pp.

Peterson, R. G., 1985: Drifter trajectories through a current meter array at Drake Passage. *J. Geophys. Res.*, **90,** 4883–4893.

Price, J. F., 1983: Internal wave wake of a moving storm. Part I: Scales, energy budget and observations. *J. Phys. Oceanogr.*, **13,** 949–965.

Weller, R. A., and R. E. Davis, 1980: A vector measuring current meter. *Deep-Sea Res.*, **27A,** 565–581.

White, W. B., and G. McNally, 1987: Evanescent pressure gradient response in the upper ocean to subinertial wind stress forcing of finite wavelength. *J. Phys. Oceanogr.*, **17,** 1032–1043.

Wyrtki, K., 1975: Fluctuations of the dynamic topography in the Pacific Ocean. *J. Phys. Oceanogr.*, **5,** 450–458.

Zubov, N. N., 1947: Dynamic oceanology. *Wind and Movement of Ice,* Engl. Transl. *Gidnometeoizdat,* 336–353.